FACULTY OF INFORMATION TECHNOLOGY AND ELECTRICAL ENGINEERING
DEGREE PROGRAMME IN ELECTRONICS AND COMMUNICATIONS ENGINEERING

MASTER'S THESIS

MODELING ANALOG SIGNAL ROUTING FOR WIDEBAND MMW PHASED ARRAYS

Author	Syed Hamza Nadeem
Supervisor	Aarno Pärssinen
Second examiner	Nuutti Tervo
Technical supervisor	Muhammad Yasir Javed

June 2022

Nadeem S. (2022) Modeling analog signal routing for wideband mmW phased arrays. Faculty of Information Technology and Electrical Engineering, Degree Programme in Electronics and Communications Engineering, 40 pages.

ABSTRACT

Modern communication systems look for higher operating frequencies to find more bandwidth to enable higher data rates. At a same time, these systems use larger and larger antenna arrays to compensate for the increased propagation losses by using antenna directivity. Often these systems use phased array approach for realizing steerable beam patterns. In phased arrays, the signal is usually divided in analogue domain to multiple transmit paths and combined in analogue domain from multiple receive paths. In this thesis, the aim is to generate a wideband modelling approach for analog signal routing in phased array transceivers that use radio frequency (RF) beamforming. In particular, the aim is to model the transfer functions of different signal paths from the sum node of all paths to the individual antennas and finally to the free space, to form a three-dimensional beam pattern that has frequency selective beam squint. The modelling approach and their behaviour in different symmetric and asymmetric beamforming architectures are presented and the performance of the system is observed through simulations by using beam patterns and equivalent amplitude responses in different directions. The impacts of array size, steering angle, and relative bandwidth are studied for the observed beam squint with different signal routing architectures to find their bandwidth limitations in different scenarios. The routing model also includes the impact of the dielectric materials of the circuit implementations.

Keywords: antenna array, asymmetric routing, beamforming, beamsteering, beam squint, frequency dependency, millimeter-wave, multi-beam system, wideband

CONTENTS

FOREWORD

This thesis is written for my Masters degree in Wireless Communications Engineering at the University of Oulu, Finland. The subject of this thesis is related to different antenna routing schemes and the effects of changing conditions and parameters for an antenna array.

First of all, thanks to Allah Almighty for granting me the strength that enabled me to complete this thesis. I would like to thank all the people who provided me their utmost support throughout my thesis. I would like to thank Professor Aarno Pärssinen for providing me this opportunity to research and work on such an advanced topic. I would like to express my deepest regards to my second examiner Dr. Nuutti Tervo for providing me with utmost support in my work and for providing guidance which, as a new researcher, I was blessed to have. I would like to take this opportunity to express my deepest gratitude to my technical advisor MSc. Muhammad Yasir Javed for supporting and motivating me throughout my thesis work.

Furthermore, I would like to thank all the Centre for Wireless Communications staff, my parents, family and friends for their support and love. A special thanks to my dearest friends Irfan, Zeeshan, Asfand and Ibrahim who have acted as my second family, away from home, in Oulu.

Oulu, Finland June 27, 2022
Syed Hamza Nadeem

LIST OF SYMBOLS AND APPREVIATIONS

5G	fifth generation
AF	array factor
dB	decibel
dBm	decibels relative to milliwatt
GHz	gigahertz
LNA	low noise amplifier
mmWave	millimeter wave
MRC	maximum ratio combining
RF	radio frequency
RMS	root mean square
ULA	uniform linear array

f_c	center frequency
$\vec{h}$	channel vector
k_x	x-component of wavevector
k_y	y-component of wavevector
k_z	z-component of wavevector
l_i	path length w.r.t other elements in a package
N_p	number of elements in package
P_{loss}	power loss
$P_{mainlobe}$	peak power of the main lobe
$P_{steeringangle}$	power at the position of the steering angle
r_n	relative placement of nth antenna from origin
τ	delay
$\vec{w}$	beamforming vector

c_0	the speed of light in free space
e_r	permittivity of the medium
u_r	permeability of the medium
λ	wavelength
π	ratio of a circle's circumference to its diameter
θ	elevation angle in spherical coordinate system
θ_s	steering angle

1 INTRODUCTION

Second phase fifth generation (5G) systems [1] and future sixth generation (6G) systems [2] use high center frequencies to achieve wider bandwidth and higher data rate. 5G systems are already using millimeter-wave (mmW) frequencies, while 6G systems aims for even higher [3]. Using higher frequencies means smaller antenna elements and increased path loss. Hence, more antennas and antenna gain are required to achieve decent link range. Due to the smaller antenna elements, mmW systems enable to pack two-dimensional (2D) antenna tiles to rather small physical size such that they can be fitted even to a handheld panel [4].

Using large antenna arrays makes the beams more directive [5]. Hence, to maintain a good signal level in mobile user scenarios, the system must configure the direction of the radiation main lobe by beamsteering. In mmW region, the antenna arrays are often implemented as phased arrays. The beamsteering is performed by phase-shifting the individual signal paths such that the signals combine coherently in/from the desired steering direction [6]. Usually the signal is routed in analogue domain in the operating frequency from/to the common sum node of all paths to/from the individual antenna elements. The outcome of dividing and combining signals in high frequency is that the signal relative bandwidth can be decent and the number of complicated signal components can be kept relatively low. This reduces the power consumption compared to so-called fully digital beamforming architecture where each antenna has individual radio frequency (RF) chain, containing also wideband digital to analog converter (DAC) and analog to digital (ADC) converters that consume significant amount of power in wideband systems [7]. On the contrary, in phased arrays, the signal loss of each path may be rather high which makes it challenging to design the paths for physically large arrays.

Millimeter-wave systems are usually designed to be wideband. This is not only because there is more bandwidth available, but also because higher center frequencies makes the relative bandwidth smaller for a given fixed bandwidth. On the other hand, the relative bandwidth may be also rather large, even in a order of 5-10% or higher in the extreme scenarios. For example, wireless local area systems operating at 60 GHz band has almost 8 GHz of bandwidth available [8]. Using very wideband signals in phased array systems is sensitive for a phenomenon called beam squint [9]. This means that the different frequency components of the input signals are pointing to slightly different directions. Especially in large arrays, this cause challenges due to the fact that the beamwidth is narrow. Due to that, the signal level in a given steering angle is strongly decreasing for the frequency components further away from the center frequency, f_c. This causes power loss to the overall received signal and is one of the reasons for the bandwidth limitations of the phased arrays. The problem is worse in large steering angles and thus the bandwidth also limit the achievable steering range of a phased array implementation.

Usually the signal division and combination is done by using passive or active power dividers/combiners and symmetric feeding network. When designing a system, signal routing has to be taken into consideration such that size, complexity and cost of the system are optimum and signal degradation is avoided which may result due to impedance mismatching. Symmetric means that the signal delay from the common node to the individual elements is the same for all antenna paths. This makes the beamsteering capabilities also symmetric to positive and negative steering angles and helps to maintain similar frequency responses in all paths. Asymmetric routing includes all scenarios where the delays of the antenna paths are not equal. Asymmetric routing as compared to symmetric routing reduces hardware area, complexity and thus cost. This is because with symmetric routes, the path lengths from all antenna elements to the summing node are equal, which leads to a greater overall path length and therefore, a greater size of the panels as compared to panels where asymmetric routing takes place. Asymmetric routing, however, introduces phase shifts among the paths since the paths are unequal and when summed at the summing node, they do not add in-phase, even if the wavefront is arriving from boresight.

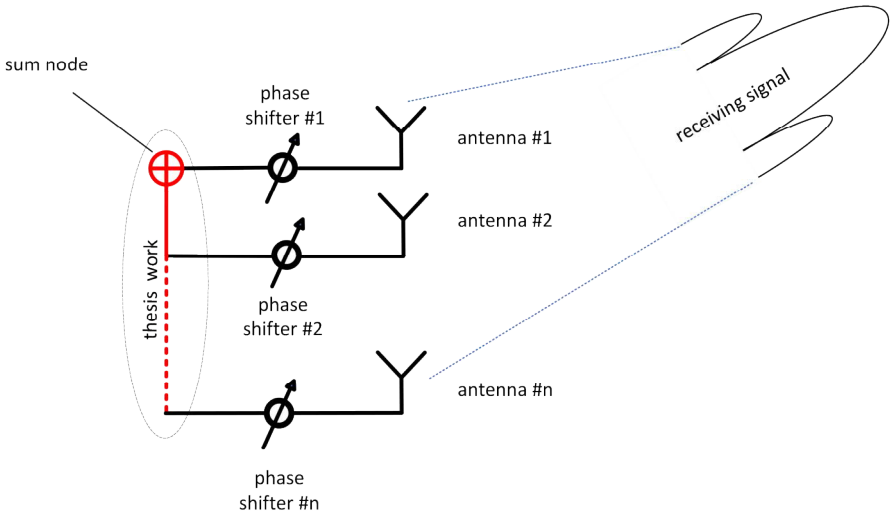

Figure 1.1. Scope of the thesis is to study and model the asymmetric analog signal routing for a broadband system.

With asymmetric routing, phase shifts among different antenna paths is an issue when they are to be combined together. Dealing with phase shifts leads to beam pointing error in different frequencies which has different responses with different steering angles and leads to bandwidth limitations.

Antenna panels are to be designed such that a multiantenna system is created where delay and phase changes arising due to different path lengths from each antenna are minimized. For this, the effects of different combinations of antenna routes with different physical parameters in a multiantenna system are carried out and studied.

There can be many different combinations to antenna routing schemes ranging from completely symmetric to different asymmetric routing comprising of different path lengths. In symmetric routing, the antenna elements or more specifically, the paths of signals from antenna elements to the sum node have equal electrical lengths. In asymmetric routing, it is not the same which leads to delay and phase changes. Simulations are carried out with these different combinations of path lengths.

Effects with a single frequency are observed for an ideal scenario, but in reality, there is always a bandwidth associated with data transfer and signal modulation. When dealing with a band of frequencies, issue of squinting arises which also has to be countered. Squinting is a phenomenon which shifts the different frequency components (angular shift) in a bandwidth, thus decreasing the wideband signal power when the steering angle is increased, when speaking in terms of the main lobe of the signal. Antenna array size also plays an important role in the signal spectrum. Increasing or decreasing the number of antenna elements affects the signal spectrum as well.

In this thesis, the aim is to model and simulate analog signal routing in phased array transceivers that use radio frequency beamforming. For the sake of clarity, the simulations and notations are given for receiver mode only, but note that the reciprocal approach can be derived also for the transmitter side.

In the following chapters of this thesis, first the concept of phased arrays and beam squint is explained and how beam squint is affected by different simulation parameters. The chapter after that explains the difference in symmetric and asymmetric routing, followed by a chapter which compares different routing scenarios.

2 PHASED ARRAY TRANSCEIVERS AND BEAM SQUINT

Phased arrays are currently the dominant technology for realizing beamforming in mmW frequencies. One of the phenomena that limits the wideband beamsteering capability of phased arrays is a phenomena called beam squinting. In this Chapter, the fundamentals of phased array based beamsteering are presented and the traditional figures of merit of the array relevant for this thesis are introduced. Furthermore, the concept of beam squint is introduced.

2.1 Phased arrays

A phased array is a type of antenna array where each antenna element is to be fed with varying phase shifts to steer the beam in different directions. Beam steering is needed to receive maximum signal power from the direction the signal is arriving to the receiver, and focus power to the direction of the receiver from transmitter. There are two main types of antenna beam steering: mechanical and electronic [10]. Mechanical beam steering is achieved by driving a directive antenna array, for instance, by using servo motors. This occurs in cases of antenna array radars like on a boat radar which is used to detect land, rainstorms, or related hazards. Electronic beam steering is achieved by changing the relative phases or delays of the RF signals in each antenna element path. This makes electronic beam steering of the antenna pattern possible. The delay or phase can be tuned either in digital or analog domains, i.e., in receiver after the ADC for the waveform samples or digital symbols, or in RF by using phase shifters or controllable delay elements [11]. In mmW frequencies, this is typically done by a phase shifter assigned to each individual antenna element. In this thesis, the focus is on the analog beamforming, i.e., phased arrays, that is more practical in mmW cellular systems designed for normal consumer use. However, similar analogy in principle works for digital beamforming as well.

Figure 2.1 shows an example schematic view of a traditional phased array receiver. In principle, the array consists of number of antenna elements, each associated with a low noise amplifier (LNA) and a phase shifter. After the phase shifters, the signals are combined. Combining will amplify the signal if the signals in each path before summation have coherent phase. The noise, that is typically uncorrelated between the antenna paths, adds up in root-mean-square (RMS) sense [12]. In overall, this will produce a beamforming gain to the signal to noise ratio (SNR) in the receiver. The signal is received at a steering angle of θ degrees and the inter-element spacing is $\lambda/2$, where λ is the wavelength of the wave at the operating frequency.

Antenna array beam is typically derived by using so-called array factor [13]. Array factor is a function of the position of the antennas in the array and derives the beam for a array of omnidirectional and isotropic point sources. For a given operating frequency and azimuth angle ϕ, and elevation angle θ, the array factor can be derived as

$$\mathrm{AF}(\phi, \theta) = \sum_{n=1}^{N} e^{-j\vec{k}(\phi,\theta)\cdot\vec{r}_n}, \tag{2.1}$$

where N is the total number of antenna elements in the array, $\vec{r}_n$ is the relative placement of nth antenna from the origin. Wave vector $\vec{k}$ describes the phase variation of a plane wave [14], in three orthogonal directions (x, y, and z-axes typically) as

$$\vec{k}(\phi, \theta) = (k_x, k_y, k_z) = \frac{2\pi}{\lambda}(\sin\theta\cos\phi, \sin\theta\sin\phi, \cos\theta).\cdot \tag{2.2}$$

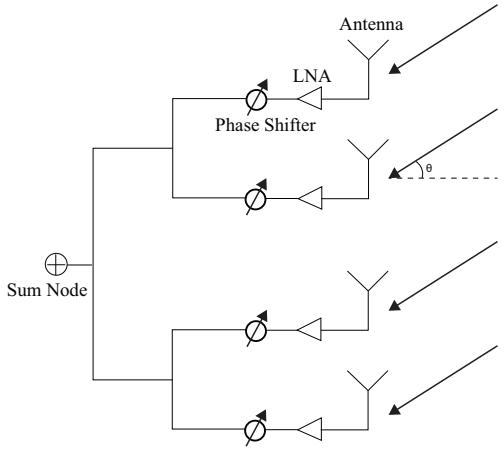

Figure 2.1. A symmetric phased array with 4 antenna elements, phase shifters and LNAs, receiving a signal at a steering angle of θ degrees.

In this thesis, work is done for a uniform linear array (ULA) considering only the z-axis, so the wave vector employed can be simplified to

$$\vec{k}(\theta) = k_z = \frac{2\pi}{\lambda} \cos\theta. \tag{2.3}$$

2.1.1 Beam steering by controllable phase shifters

In phased arrays, the beam steering is performed by digitally controlled phase shifters, connected to each antenna element. The aim of the steering is to change the plane (direction) in which the signals arriving to each antenna element are combined coherently when the paths are summed together. Coherent means that the phases of the signals are the same when they are summed. The complex valued beamforming coefficients to steer the beam to a given steering angle θ can be derived by using so called maximum ratio combining (MRC)[15]. Easiest way to derive this is to use the equation (2.1). Often in beamforming, we note the phase and amplitude of each element by using typical radio channel notations. Hence, the (2.1) for ULA aligned in z-axis can be rewritten as

$$\mathrm{AF}(\theta) = \sum_{n=1}^{N} e^{-j\vec{k}(\theta)\vec{r_n}} = \sum_{n=1}^{N} h_n(\theta) = \vec{w}\vec{h}(\theta), \tag{2.4}$$

where $\vec{h}(\theta) = [h_1, h_2, ..., h_n]^T$ denotes channel in each antenna element for a wavefront arriving from angle θ. Vector $\vec{w}$ can be denoted as beamforming vector, which in case of no beamsteering contains only ones as $\vec{w} = [1, 1, ..., 1]$. Hence, the MRC, or in this case, beamstreering coefficients, can be derived simply as

$$\vec{w} = \vec{h}^H, \tag{2.5}$$

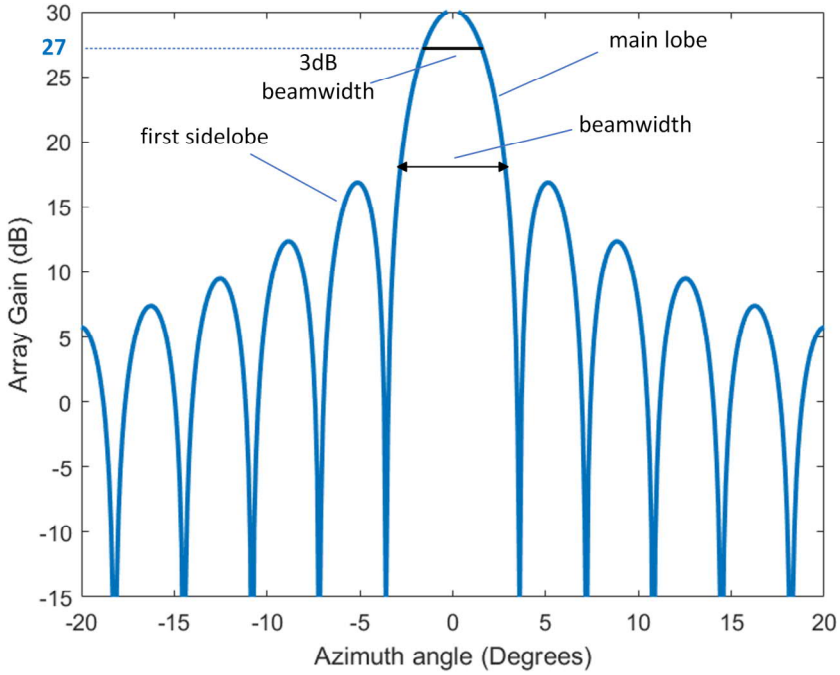

Figure 2.2. Antenna radiation pattern for a directional antenna with an array of 32 antennas operating at 30 GHz.

where $(\ )^H$ is the conjugate transpose. Now the array factor in the steering angle with ideal beam steering is

$$\mathrm{AF}(\theta, \theta_s) = \vec{w}\vec{h}(\theta) = \sum_{n=1}^{N} e^{j\vec{k}\vec{r_n}} e^{-j\vec{k}\vec{r_n}} = \sum_{n=1}^{N} 1 = N, \tag{2.6}$$

where θ_s denotes the steering angle.

2.1.2 Phased array figures of merit

Figure 2.2 shows an example radiation pattern for a ULA of 32 antennas. The main lobe is the direction where the antenna array receive maximum signal power with clearly visible beam. Without any active beamsteering, ULA has a main lobe at 0°. In antenna systems, some typical figures of merit are often used to describe the shape of the beam. These are, for example, main lobe gain, beamwidth and sidelobe level. Beamwidth is defined as the width of the main lobe of the antenna radiation pattern, or in other words, the area (in degrees) over which the main lobe is spanned and the majority of the beam power is radiated. 3dB beamwidth is the beamwidth of the main lobe where 50% of the peak power of the main lobe radiates. In the direction of the first side lobe, in either side of the main lobe, the power level is ideally around 13 dB less than the peak of the main lobe. This is called as sidelobe level. The value of around 13 dB is achieved when all antenna elements are exited with same amplitude and the phase is is progressively chaining over the elements with fixed spacing. As we go further away from the main lobe, the side lobe level keeps on decreasing. The total number of lobes, including the main lobe are equal to $N - 1$ where N is the number of antennas in the array.

Antennas are usually designed for a certain operating frequency with a desired operational

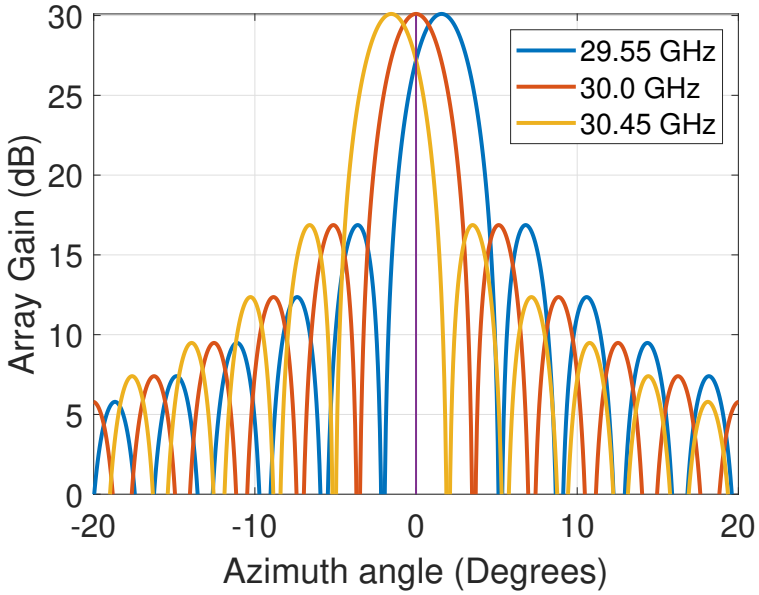

Figure 2.3. Antenna radiation pattern for a directional antenna with an array of 32 antennas, with three frequencies covering 3% relative bandwidth around 30 GHz.

bandwidth. For an antenna, the bandwidth is often defined based on the antenna matching, i.e., reflection coefficient, or based on realized gain of the antenna. In this thesis, the focus is on beamforming part and thus we assume that antenna elements themselves are ideal and capable of radiating signal in all frequencies. Hence, the frequency-selectivity of the system is only based on antenna array configuration and its feeding network, which is seen as a frequency selectivity in the realized beam. In Figure 2.2, beam of only a single frequency is received on the antenna array. Figure 2.3 shows the simulation result with the same parameters as in Figure 2.2, except now the relative bandwidth of 3% of 30 GHz is used, that is, from 29.55 GHz to 30.45 GHz. Three frequency points are taken to demonstrate results. With frequencies other than the center frequency (30 GHz), the signal beam is formed at a shifted angular position. This phenomenon is called squinting which is covered in Chapter 2.2. The higher frequency beam shifts to the left and the lower frequency beam shifts to the right.

2.2 Beam squint in traditional phased arrays

In phased array system, phase shifter values are selected based on the frequency of interest, antenna configuration and steering angle. This means that phase shifters are often used instead of ideal delay shifts and each frequency undergoes different phase, steering the beam to slightly different directions. This is caused by the fact that with respect to the planar wavefront propagating to a certain direction, the path length from the plane to each antenna (or vice versa) is slightly different. By rewriting the wave-vector **k** (number) in equation (2.3) as a function of frequency instead of bandwidth this can be modeled as

$$\mathrm{AF}(\theta, f) = \sum_{n=1}^{N} e^{-j\vec{k}(\theta,f)\vec{r_n}} = \sum_{n=1}^{N} h_n(\theta, f) = \vec{w}\vec{h}(\theta, f), \tag{2.7}$$

where f is the frequency and

$$\vec{k}(\theta, f) = \frac{2\pi f}{c_0} \cos\theta, \tag{2.8}$$

where c_0 is the speed of light (wave) in free space. Now the equation (2.7) will produce different array factor in each frequency.

2.2.1 Delay vs phase shift for large arrays

In practice, the beam squint phenomena is related to the fact that the delay is not the same as phase shift, or in other words, phase shift approximates the delay only at a certain frequency. Hence, when the wave is traveling a certain physical (electrical) distance, the experienced phase shift is different for every frequency component. Generally, two different phase-delay relations are used in the electrical circuit modeling: phase delay and group delay. Group delay is the rate of change of phase with respect to the angular frequency $2\pi f$ [16] and can be derived as

$$\tau_{group} = -\frac{\partial\phi}{2\pi\partial f}, \tag{2.9}$$

where ϕ is the phase and ∂ denotes the derivative with respect to the frequency f. Phase delay is the phase angle at that particular frequency and can be written as

$$\tau_{phase} = -\frac{\phi}{2\pi f}. \tag{2.10}$$

The relation above causes the beam main lobe to deviate from the desired direction in different frequencies. Each antenna element in an array receives signals at a different time instant. At the point of combining, that is, at the sum node, these signals will not be combining fully coherently over the whole bandwidth.

2.2.2 Beam pointing error of the main lobe

The beam pointing error is introduced when the antenna array beam points in the direction other the steering angle. The error is defined as the difference between the position of the beam's main lobe in degrees and the steering angle.

A beam pointing error indicates that the antenna radiation power is not received in the direction it is supposed to, that is the direction in which the receiver antennas are. Beam pointing error causes loss in the power. For a wideband system each frequency component has different beam pointing error, which means that in the actual desired angle, the received power varies over frequencies. This decreases the overall wideband signal power and it also challenges the data detection. This is a bigger problem with larger antenna arrays because as the array size increases, the beamwidth decreases and even though the beam pointing error is the same, less power is received at the same angular position. With larger steering angles, the beam pointing error is greater. This is because the main lobes of different frequency beams are at a greater angular distance from the main lobe of the center frequency beam.

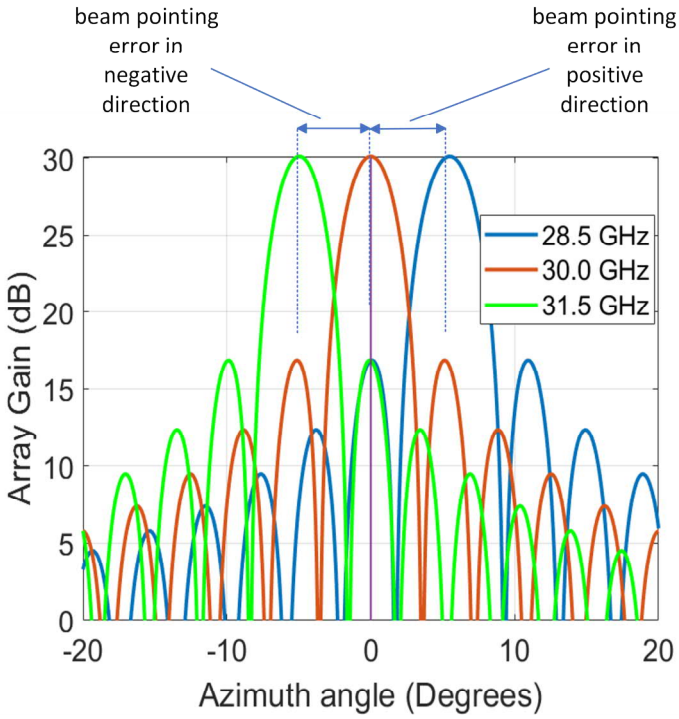

Figure 2.4. Beam pointing error of the main lobe for antenna radiation pattern for a 32 antenna array, with three frequencies covering 10% bandwidth of 30 GHz for an asymmetrically routed array.

2.2.3 Trade-off between array size, bandwidth, and steering angle

Power loss is calculated as the difference between the peak power of the main lobe at a particular frequency and the power level of the same main lobe at the steering angle position at the same frequency. Power loss is calculated as

$$P_{loss} = P_{mainlobe} - P_{steer}, \tag{2.11}$$

where $P_{mainlobe}$ is the main lobe power while the P_{steer} is the power at the desired steering angle, that may be different from the main lobe.

Changing the antenna array length does not affect the beam pointing error as can be seen from Figures 2.5(a), 2.6(a) and 2.7(a). However, it does affect the power loss in the beam. An array consisting of greater number of antennas experiences greater power loss within the same bandwidth as compared to an array with fewer antennas. This is because increasing the number of antennas decreases the beam width and increases the peak power and hence even a small beam pointing error causes a significant power loss at a specific steering angle. The, power loss increases as the antenna elements are increased as can be seen from Figures 2.5(b), 2.6(b) and 2.7(b).

Steering angle or the scan angle is the angle in which the beam is to be steered. In this thesis, only receiver side is being considered for the sake of clarity. So when the beam steering is altered, that is, changed from azimuth angle of 10°, squinting occurs in terms of power loss and beam pointing error for a particular beam bandwidth. At 10°steering angle, the beam pointing error increases as we go further away from the center frequency as shown in Figure 2.7(a).

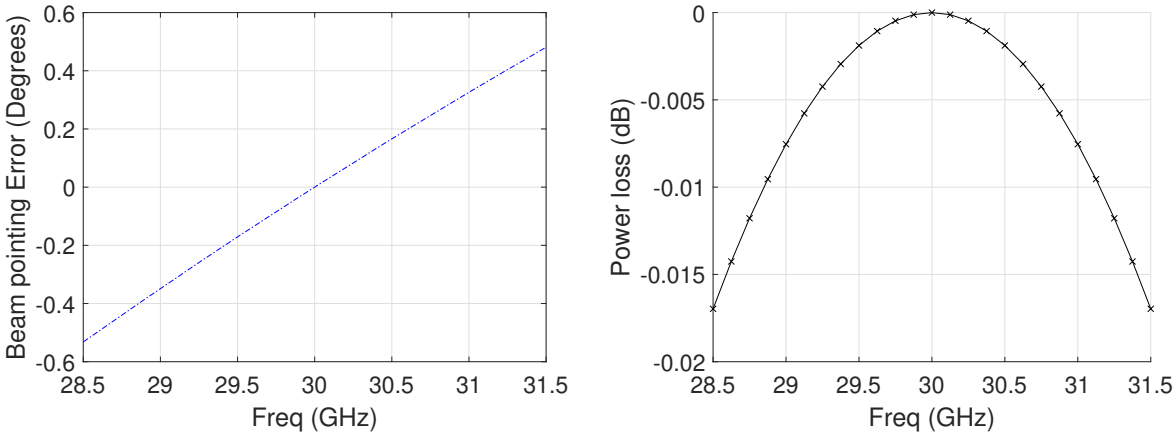

(a) (b)

Figure 2.5. (a) Beam pointing error of the main lobe for antenna radiation pattern for an 8 antenna array, at a 10% bandwidth of 30 GHz at 10°steering angle for symmetric routing and (b) Power loss experienced at the main lobe.

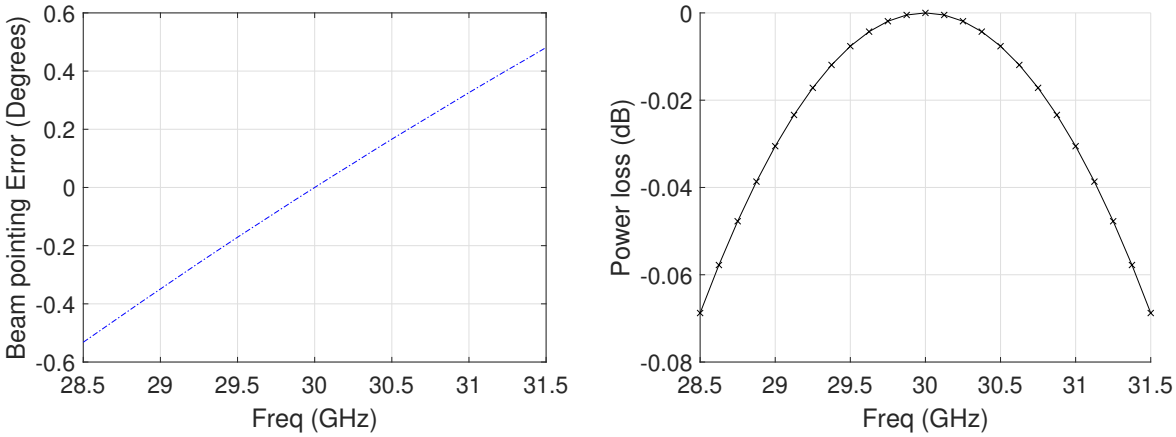

(a) (b)

Figure 2.6. (a) Beam pointing error of the main lobe for antenna radiation pattern for a 16 antenna array, at a 10% bandwidth of 30 GHz at 10°steering angle for symmetric routing and (b) Power loss experienced at the main lobe.

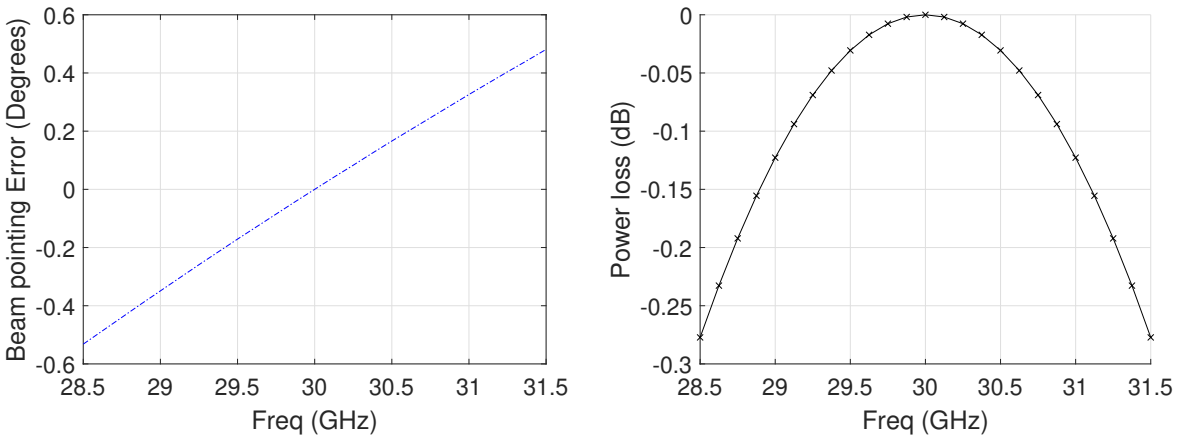

(a) (b)

Figure 2.7. (a) Beam pointing error of the main lobe for antenna radiation pattern for a 32 antenna array, at a 10% bandwidth of 30 GHz at 10°steering angle for symmetric routing and (b) Power loss experienced at the main lobe.

It shows a similar pattern with -10°steering angle as shown in Figure 2.9(a). At 0°steering angle, the beam pointing error is equal to zero at all frequencies. At 20°steering angle, the beam pointing error increases as shown in Figure 2.10(a). This shows that entire beams shift according to the steering angle. As the steering angle increases, power loss decreases as can be seen from Figures 2.7(b), 2.8(b) and 2.10(b) where maximum power loss increases from 0 dB to 0.275 dB to 1.5 dB as the steering angle is increased.

The squinting effect is also dependent on the relative bandwidth of the signal used in the antenna array system. A greater relative percentage bandwidth faces a greater beam pointing error as compared to lower percentage bandwidth. This can be seen from Figures 2.7(a) and 2.11(a). In Figure 2.7(b), the maximum power loss is close to 0.275 dB, while in Figure 2.11(b), it is 0.025 dB which is a significant difference in power loss.

The phase shifters employed in the system, like all other phase shifters, have equal phase across different frequencies. In reality, modulated band signals have a finite bandwidth over a frequency range. This causes different frequencies in the relative bandwidth to travel to slightly different directions. When the frequency is higher than the center frequency or the frequency for which the phase shifter is designed, the main lobe shifts to the left of the steering angle. When the frequency is lower, the main lobe shifts to the right.

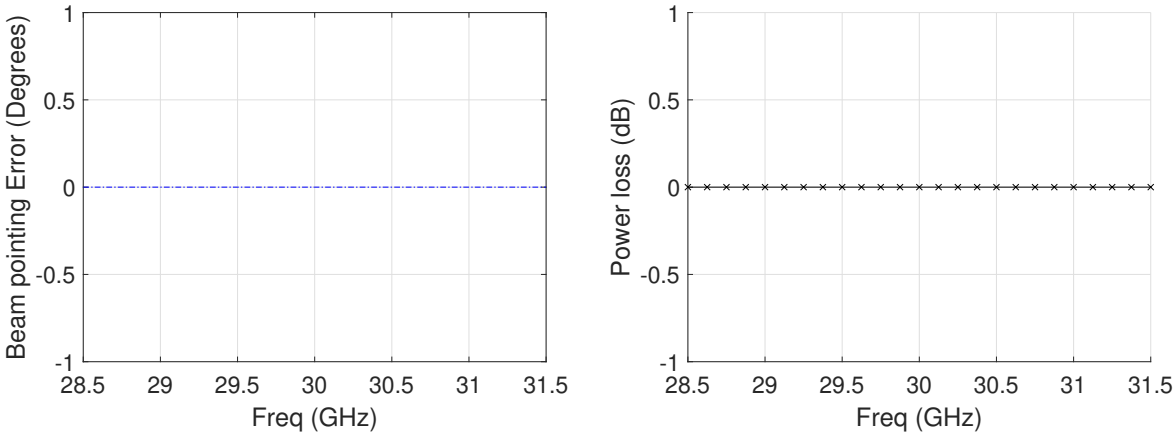

(a) (b)

Figure 2.8. (a) Beam pointing error of the main lobe for antenna radiation pattern for a 32 antenna array, at a 10% bandwidth of 30 GHz at 0°steering angle for symmetric routing and (b) Power loss experienced at the main lobe.

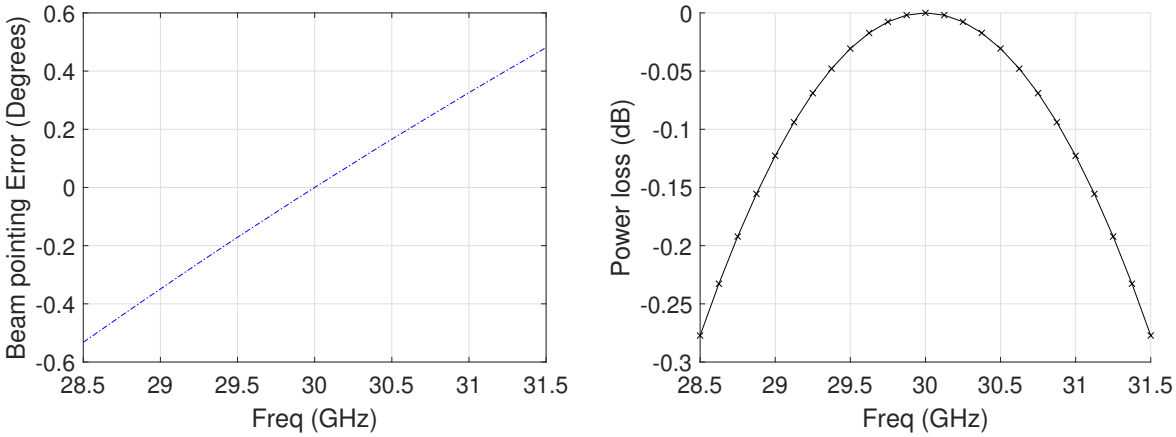

(a) (b)

Figure 2.9. (a) Beam pointing error of the main lobe for antenna radiation pattern for a 32 antenna array, at a 10% bandwidth of 30 GHz at -10°steering angle for symmetric routing and (b) Power loss experienced at the main lobe.

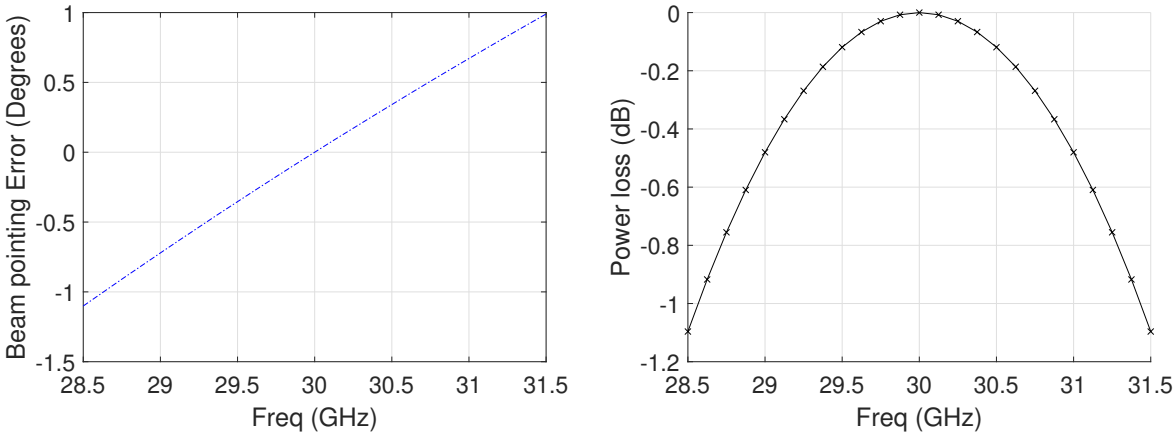

(a) (b)

Figure 2.10. (a) Beam pointing error of the main lobe for antenna radiation pattern for a 32 antenna array, at a 10% bandwidth of 30 GHz at 20°steering angle for symmetric routing and (b) Power loss experienced at the main lobe.

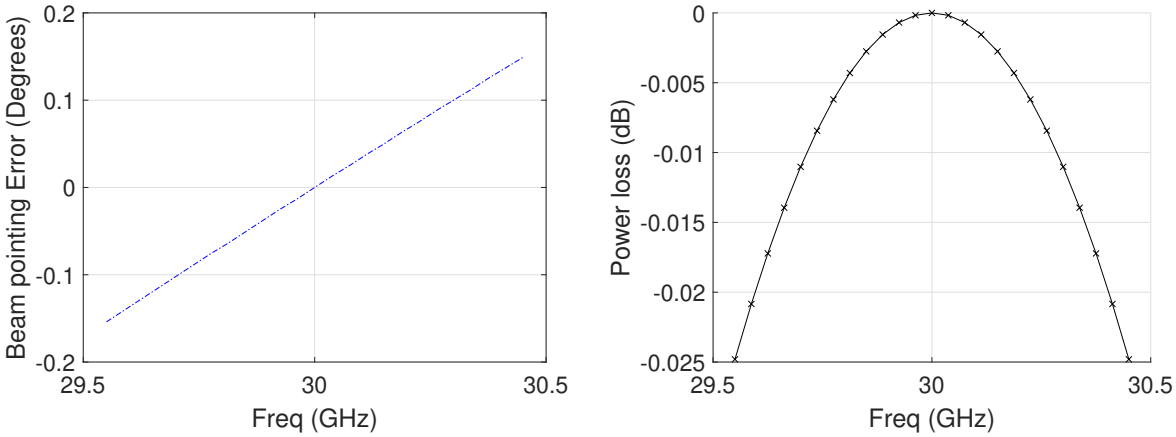

(a) (b)

Figure 2.11. (a) Beam pointing error of the main lobe for antenna radiation pattern for a 32 antenna array, at a 3% bandwidth of 30 GHz at 10°steering angle for symmetric routing and (b) Power loss experienced at the main lobe.

3 ASYMMETRIC AND SYMMETRIC SIGNAL ROUTING

In the phased array receivers, the signals received by individual antenna elements must be routed for the rest of the RF components such as mixer and analog to digital converter (ADC). Routing the signals from the digital parts to the mmW front-end and antennas is lossy and takes a lot of circuit area. Traditionally, phased array antennas are fed in such a way that the electrical lengths of different antenna paths are the same. In this thesis, this is denoted as symmetric routing scheme. The symmetric routing is used to maintain the path delays equal in order to enable wideband symmetric beamsteering over a large angular sector. The requirement of having the path lengths equal is not often questioned: instead, the symmetric routing especially for phased arrays used in communications has become a standard design choice. Nevertheless, it is interesting to look also routing schemes that are not fully symmetric. In this thesis, these scenarios, where the path lengths are not all equal, are simply called as asymmetric routing schemes. These scenarios include basically all cases where there is even one path length that is different from the others. The asymmetric signal routing has benefits related to the circuit implementation that could help to make more innovative modular circuit platforms [17] that can be used to decrease the circuit area of the paths from digital to the mmW antennas. However, asymmetry causes plenty of other challenges related to delay mismatch and asymmetry in losses that makes it challenging to achieve good wideband beamsteering and requires careful considerations and calibration schemes to overcome. In this chapter, we introduce how to model the delay in various signal routing solutions. The symmetric scenarios are given as a reference, while the focus is on the asymmetric scenarios [17].

3.1 Symmetric routing

In symmetric solutions, the routing is often internally implemented by combining two paths at a time in a tree-like formation. The power combiners (receiver mode) are placed such that the path lengths from different antennas are kept constant. For the plane wavefront arriving to the antenna from the boresight, this keeps also the delays of the different paths, with respect to the angle of arrival, equal. This is illustrated in the Figure 3.1 by the nominal arriving wavefront as a line parallel to the uniform linear array drawn to the figure. Another way to illustrate this is to draw the free-space equivalent relative path lengths with respect to the boresight direction. This is illustrated in Figure 3.2. The corresponding beams are given in Figure 3.3.

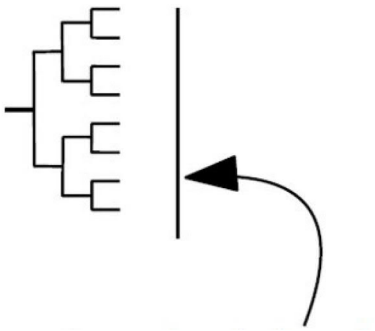

Figure 3.1. Symmetric routing scheme with the nominal planar wavefront arriving to the array. The wavefront in the figure is the wavefront that corresponds to the desired delays of the array for squint-free operation. Antenna elements are located at $\lambda/2$ distance at the center frequency.

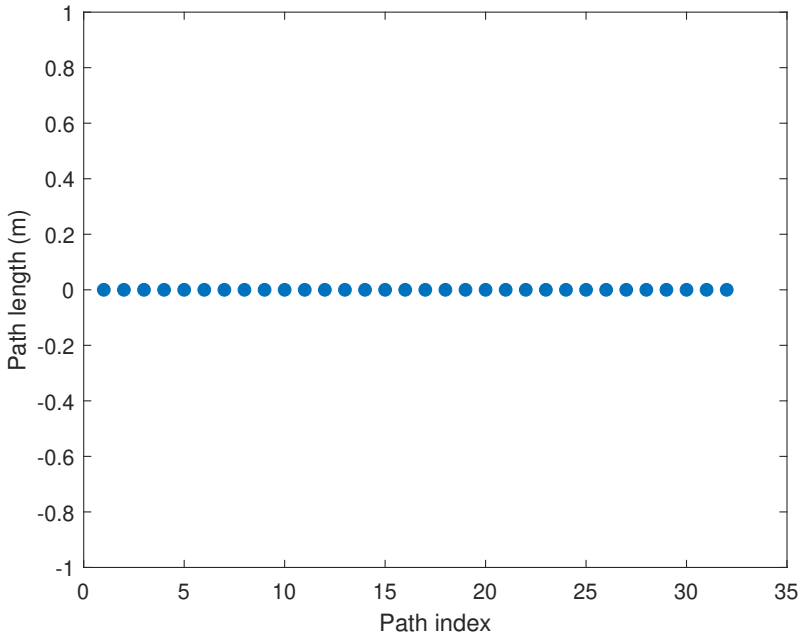

Figure 3.2. Relative free-space equivalent path lengths of the symmetrically fed 32-element uniform linear array.

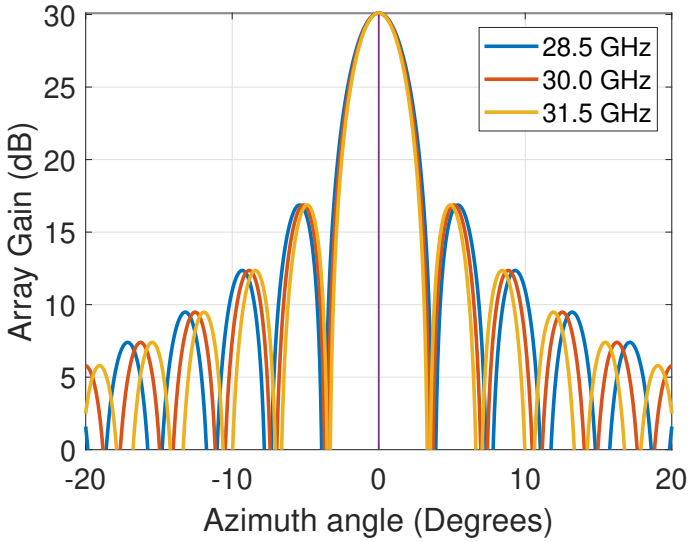

Figure 3.3. Beam shape of symmetrically routed 32-element uniform linear array, with 10% bandwidth 30 GHz frequency and with no beam steering in different operation frequencies. With symmetric routing, the beam pointing error is zero for the boresight angle or arrival.

In symmetric routing scheme, the wavefront arriving from the boresight has no squint, which means that the beam pointing error is initially zero, if assumed no delay, amplitude or phase errors in the array implementation. The slight variation over the beams outside the boresight are actually caused by the fact that the beamwidth is different for different operation frequencies for a fixed antenna array size with fixed antenna spacing derived based on a spot frequency.

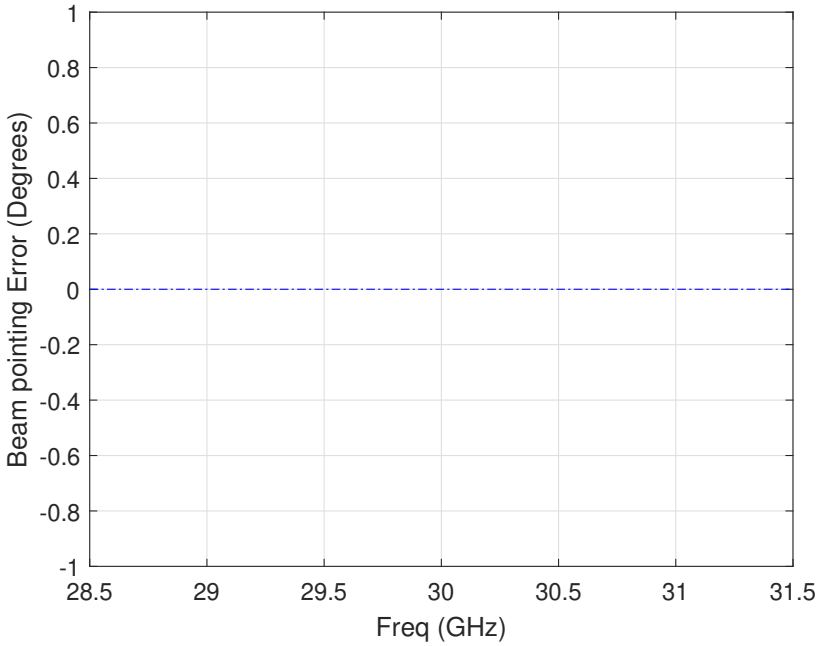

Figure 3.4. Beam pointing error with symmetric routing.

3.2 Asymmetric routing

In the asymmetric routing technique, the signal paths or routes are not equal in length. These different distances cause delay and phase changes between signals arriving from different antenna elements to the sum node. This causes the array to have beam squint even when steered towards boresight. The asymmetric routing schemes are used for example in so called end-fire arrays, where the array is fed from one corner and the path lengths are gradually increasing towards the last antenna element. Such array, if electrical path lengths correspond to the antenna spacing, nominally radiated parallel to the array: in such solutions the maximum direction of the array is towards the end of the array. Similar principles are in many fixed antenna array structures such as Yagi-Uda-types of antennas used for example in TV and Radio receivers in broadcasting systems.

3.2.1 Examples of asymmetric routing

There are in principle infinite number of configurations that have asymmetric routing. In steerable arrays, the asymmetry can be illustrated by change in the desired squint-free wavefront of the array. An example of that is illustrated in Figure 3.5. In the figure, the array is composed by 9 antennas with a sum node at the second antenna element. The antenna radiation pattern for this architecture is shown in Figure 2.4 in Chapter 2.

3.2.2 Impact of routing material used RF design

The antenna board has a different permeability and permittivity than air. As the radio waves enter the board from the air, they encounter a change in the permeability and permittivity values due to change in media. Permeability of the board is usually close to free space permeability.

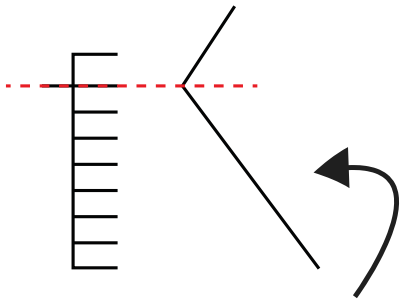

Figure 3.5. Illustration of the antenna array with asymmetric routing. In the figure, the the second antenna element is taken as the reference antenna.

Permittivity, however, is different. In this thesis, the simulations are carried out with the board permittivity value of 3.3 relative to air. The radio wave speed and wavelength reduces as it enters from air to the board and frequency remains unchanged.

Incorporating the permittivity and permeability values of the board changes the wavenumber as

$$k_{board} = \frac{2\pi\sqrt{\epsilon_r \mu_r}}{\lambda} \tag{3.1}$$

where e_r is the relative permittivity of the medium and u_r is the permeability of the medium which is taken as 3.3 in this thesis.

3.2.3 Asymmetry compensation by phase shifters

The routing delays are compensated by using phase shifters attached to each antenna element. The phase shifter equation incorporated into the system can be expressed as

$$H_{ps} = e^{j\vec{k}\vec{r}} \tag{3.2}$$

Figure 3.6 shows beam compensated and uncompensated versions. In the compensated beam, the path lengths are compensated by the phase shifters. The uncompensated version experiences vast experiences vast beam pointing error.

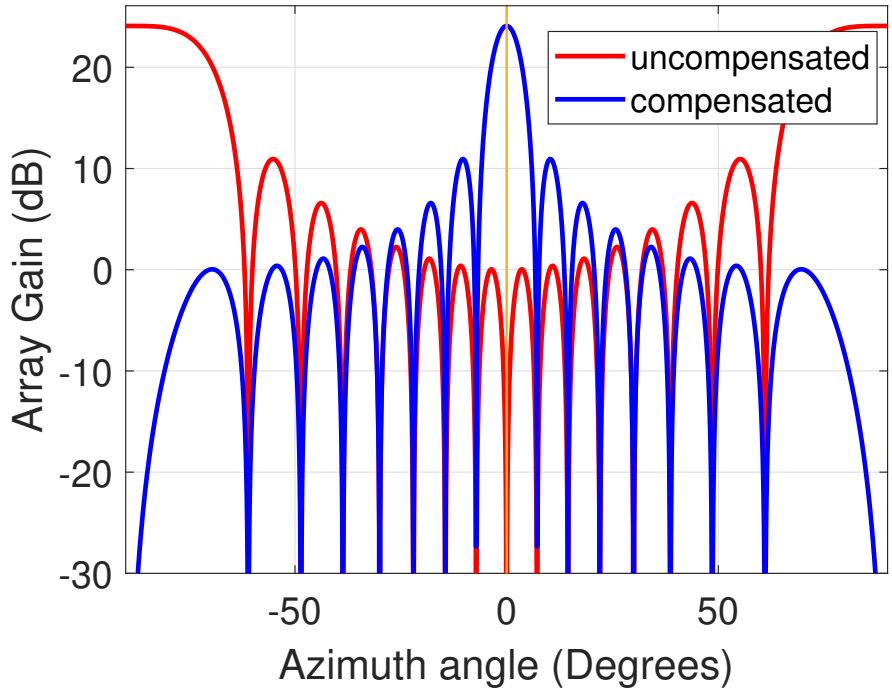

Figure 3.6. Beams of the asymmetrically fed phased array, as in Figure 3.5, with beamsteering to the boresight. 16 antenna elements are used at a steering angle of 0°, frequency of 30 GHz and the first antenna of the ULA is taken as the reference antenna.

4 COMPARISON OF THE ANALOG SIGNAL ROUTING ARCHITECTURES

As discussed in the previous section, analog signal routing can be symmetric or asymmetric. The word "asymmetric routing" here contains unlimited number of different possible routing options because there can be any possible combination of unequal paths from antennas to the rest of the circuitry in the antenna panels. However, often the physical path lengths are dependent on the overall RF transceiver design and architecture. This section discusses how different antenna paths produce different results.

4.1 Arrays with constantly increasing path lengths

These are the scenarios for the routing where a sum node to one particular antenna is positioned and the others are routed to that. All paths are asymmetric, meaning that adjacent elements are never symmetric in this architecture. Alternatives are given in subsections.

4.1.1 Phased array fed from the edge of the array

Figure 4.1 shows the antenna path length for 32 antenna array and Figure 2.4 in Chapter 2 corresponds to the antenna spectrum of this path. The setup consists of an array of 32 antennas in a straight line. Such a setup is also called a uniform linear array (ULA). The first antenna element is the reference antenna. This means that the summing node is at the first antenna element, that is, the antenna signals are summed at the point of the first antenna element of the array. It can be observed that there is definite squinting as compared to the symmetric routing spectrum in Figure 3.3 that was given in Chapter 3. In symmetric routing scenario, all the different frequencies coincide at the main lobe. However, in asymmetric routing, different frequencies have their main lobes at different angular positions.

4.1.2 Phased array fed from an arbitrary reference antenna

In Figure 4.2, the 2nd antenna element is taken as the reference antenna, that is, the summing of signals is done at the 2nd antenna of the array and power spectrum obtained as shown in Figure 4.3. It is observed that the first sidelobe level is lower with second antenna element as the reference antenna as compared to when the first element was taken as the reference.

4.1.3 Phased array fed from its midpoint

To show a big contrast in results, summing is moved from 2nd antenna element to the antenna element at the center of the array, that is the 16th element. Fig 4.5 shows that the path length for antennas is greatest for the elements that are located at the array ends and path length decreases as we move towards the center element. This is still asymmetric routing and not symmetric because the path lengths are not equal for all the elements.

Figure 4.6 is the power spectrum for this setup. It is clearly different from Figures 2.4 and 4.3 because apart from the center frequency of 30 GHz, none of the frequencies in the bandwidth (10 GHz bandwidth) reach 30 dB of array gain. Figure 4.8 shows the beam pointing error of

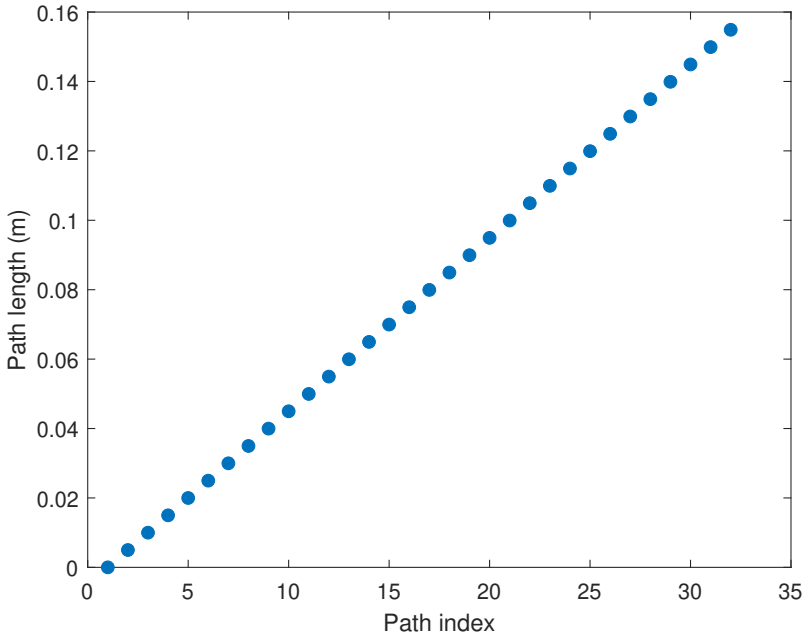

Figure 4.1. Asymmetric path routing with 32 antenna elements, steer angle 0°, beams at different frequencies and with sum node at 1st element.

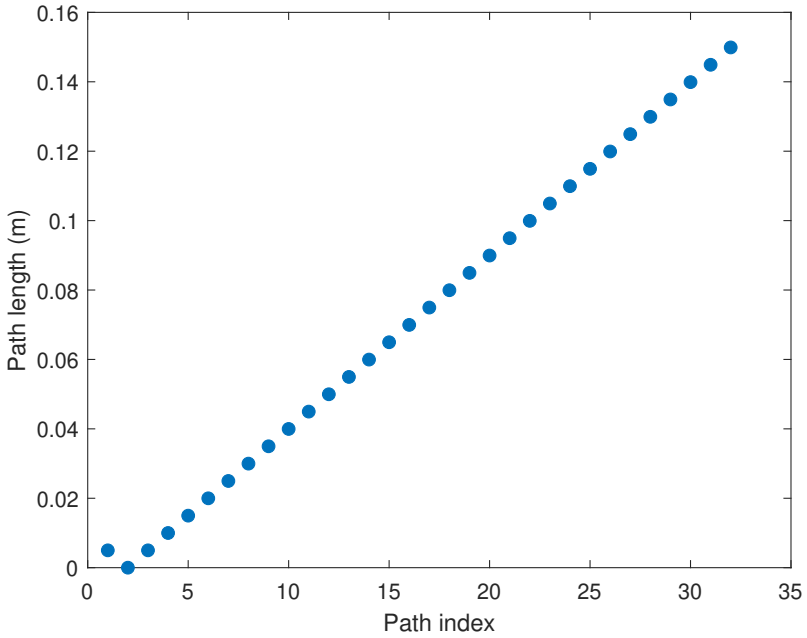

Figure 4.2. Asymmetric path routing with 32 antenna elements, steer angle 0°, beams at different frequencies and with sum node at 2nd element.

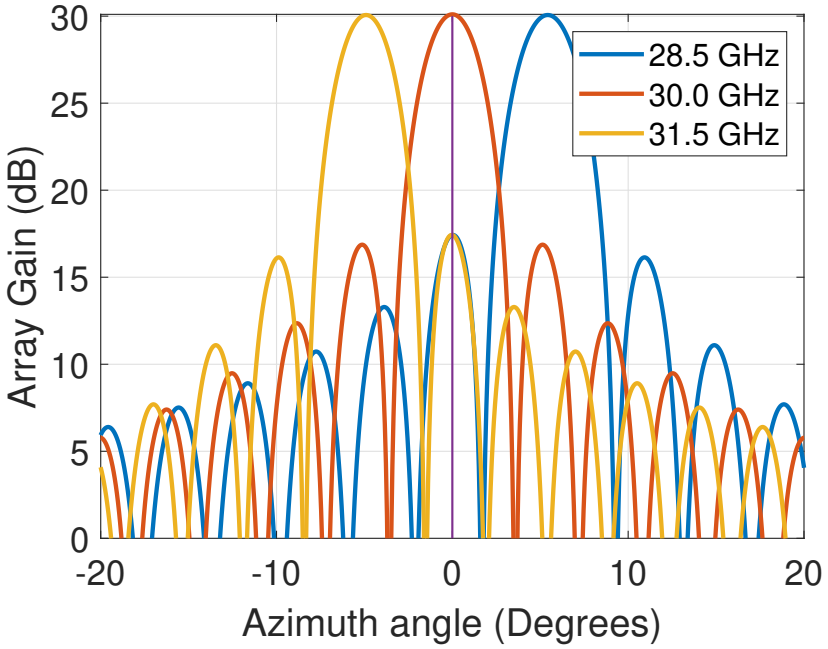

Figure 4.3. Asymmetric path routing with 32 antenna elements, steer angle 0°, beams at 3 different frequencies and with sum node at the 2nd element.

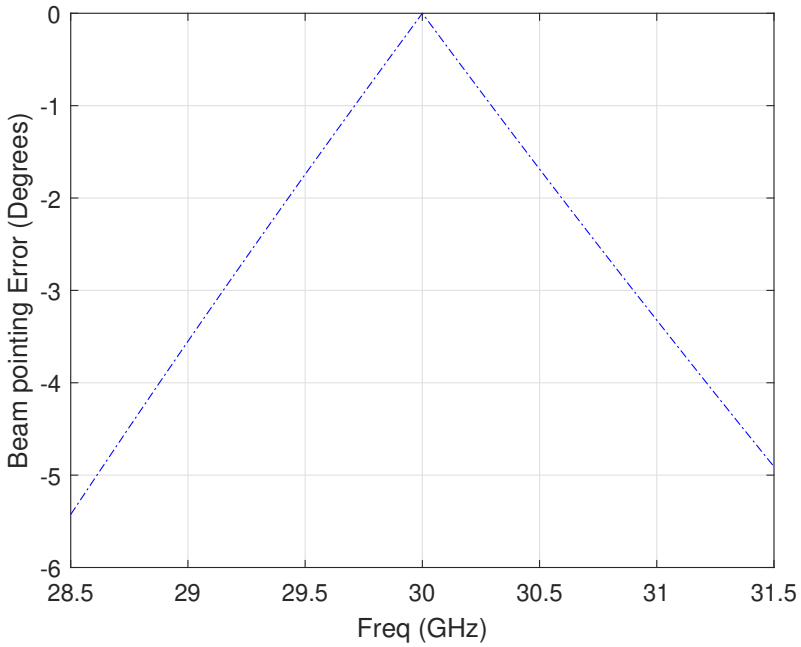

Figure 4.4. Beams pointing error with 2nd antenna element as the reference antenna

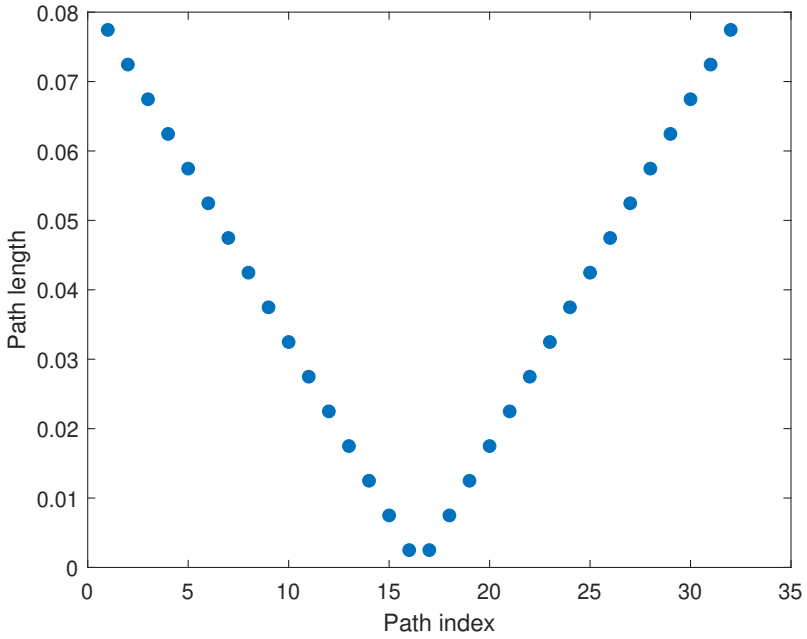

Figure 4.5. Asymmetric path routing with 32 antenna elements, steer angle 0°, beams at different frequencies and with sum node at 16th element.

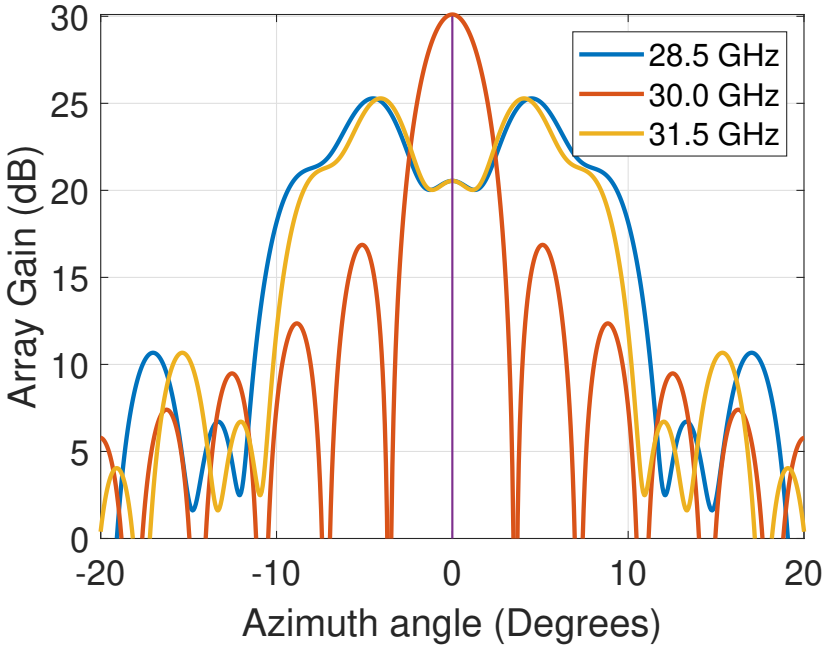

Figure 4.6. Asymmetric path routing with 32 antenna elements, steer angle 0°, beams at 3 different frequencies and with sum node at 16th element.

this setup. It can be seen that a major part of the bandwidth has zero beam pointing error. This can also be seen from Figure 4.7 where many frequency points lie at the steering angle position (which in this case is 0°), making the angular distance between the main lobes of center frequency and other frequencies equal to zero.

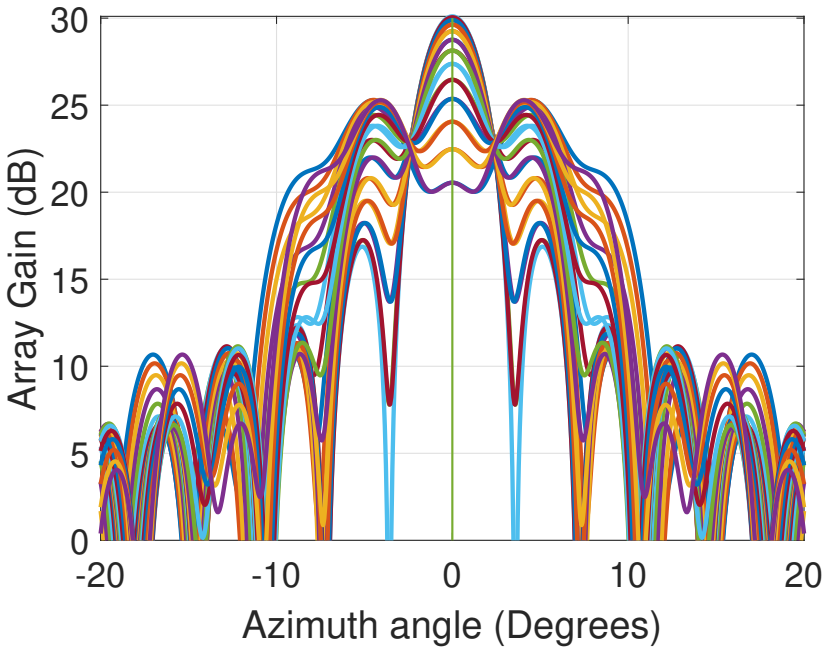

Figure 4.7. Asymmetric path routing with 32 antenna elements, steer angle 0°, beams at different frequencies and with sum node at 16th element with multiple frequency points.

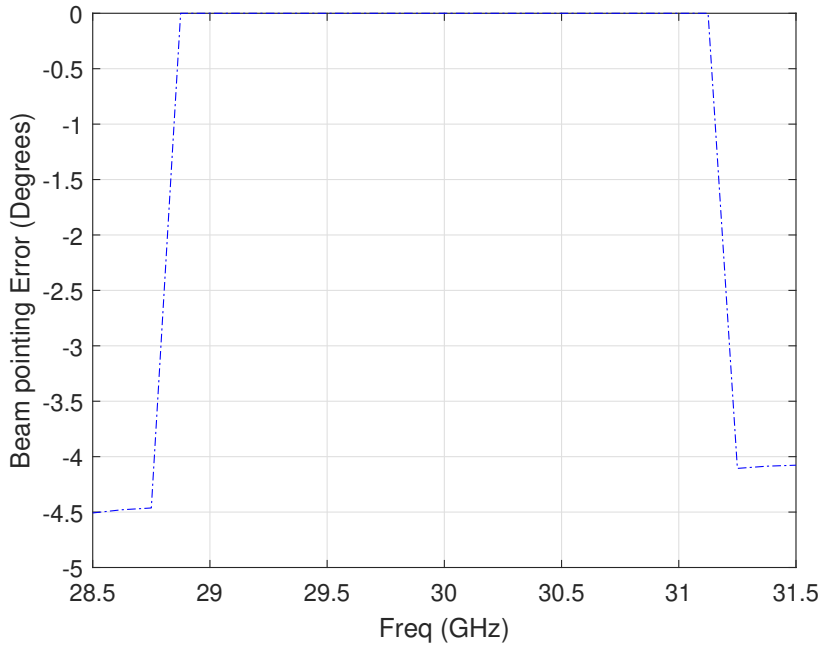

Figure 4.8. Beam pointing error with Phased array fed from its midpoint (16th antenna element).

4.2 Modular design approach for antenna panels

Another approach to arrange antennas is in the form of sub-clusters, i.e. groups of elements. In this thesis, this is called a modular routing approach. Even the modular approach can have unlimited possibilities of how the antennas are arranged and what combinations are used. Phased arrays can be arranged as sub-arrays in panels or integrated circuits. This approach to antenna arrays is cost-effective and flexible [18].

An example of 16 antennas is shown in Figure 4.9 where each package contains 4 antenna elements. The routing is symmetric inside every package since the path lengths are equal for all elements. However, the overall routing is still asymmetric because path lengths are not equal for all packages. Path lengths are equal for packages 1 and 2 and similarly are equal for packages 2 and 3, since the summing is done at the center of the whole array as shown in Figure 4.9. This also shows that asymmetric routing can be done by using symmetric routing.

In this section, a modular approach to antenna panels is applied, where previously antenna elements were placed individually.

The array of path lengths within each package is denoted as

$$\vec{L}_{sub} = [l_0 \dots l_{N_p-1}], \tag{4.1}$$

where l_i is the path length with respect to the other elements in the same package and N_p is the number of elements in the package. Similarly, the channels, i.e. frequency responses of the elements within the module can be written as

$$\vec{H}_{sub}(f) = [e^{-2\pi l_0 \frac{f}{c}} \dots e^{-2\pi l_{N_p-1} \frac{f}{c}}], \tag{4.2}$$

where c corresponds the speed of the wave at the routing media, if l_is are defined in free space. Note that if l_is are given as in electrical length, then $c = c_0$ corresponds the speed of the light in free space. The package can be either an integrated circuit or an antenna panel. The route lengths between the common sum node and the package inputs can be derived as

$$\vec{L}_{route} = [\vec{L}_{route,0}, ..., \vec{L}_{route,N_r}], \tag{4.3}$$

when the total number of antenna elements in the array is $N_p N_r$ This particular route length is for summing at the center of the array where the route length decreases from the corner of the array towards the center of the array. The simulation results shown in Figures 4.10, 4.11, 4.14

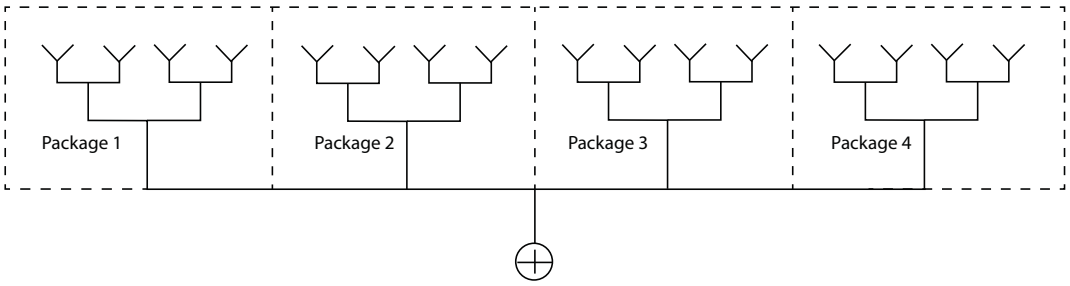

Figure 4.9. Asymmetric routing example containing antenna packages with each package containing four individual antenna elements. The elements inside each antenna sub-group are symmetrically exited.

and 4.15 and all have summing node at the center. The frequency responses of the routing paths that combines the modules can be now derived as

$$\vec{H}_{route}(f) = [e^{-2\pi\vec{L}_{route,0}\frac{f}{c}} \dots e^{-2\pi\vec{L}_{route,n}\frac{f}{c}}], \tag{4.4}$$

where $\vec{L}_{route,0}, ..., \vec{L}_{route,n}$ are the lengths of the signal paths from the module outputs to the common sum node. The overall channels from every antenna to the sum node can be derived as

$$H_{tot}(f) = \vec{H}_{route}(f) \otimes \vec{H}_{sub}(f), \tag{4.5}$$

where $\otimes$ denotes the Kronecker product of the the two matrices containing the fractional path lengths. The Kronecker product of dimensions *mc* x *nd* is defined as the product of two matrices M1 and M2 where M1 is *m* x *n* and M2 is *c* x *d* [19].

4.2.1 Asymmetric routing for symmetric antenna modules

Groups of 4 antenna packages are arranged asymmetrically in an array as shown in 4.10. The individual elements inside a package have a symmetric arrangement since their path lengths are equal from the summing node. However, the overall arrangement is asymmetric because the path length of the packages is not the same from the summing node. The signal array gain is simulated as shown in Figure 4.11 and with the same simulation with multiple frequencies is shown in Figure 4.12. The presence of multiple main lobes at the steering angle position (at 0°) again shows why the beam pointing error is zero in many frequency range as shown in Figure 4.13.

Figure 4.14 shows the path length against path index for antenna elements in pairs. Figure 4.15 shows the array gain simulation for this setup and Figure 4.16 shows its corresponding beam pointing error. Here the main lobe of all frequency components except the center frequency are approximately the same.

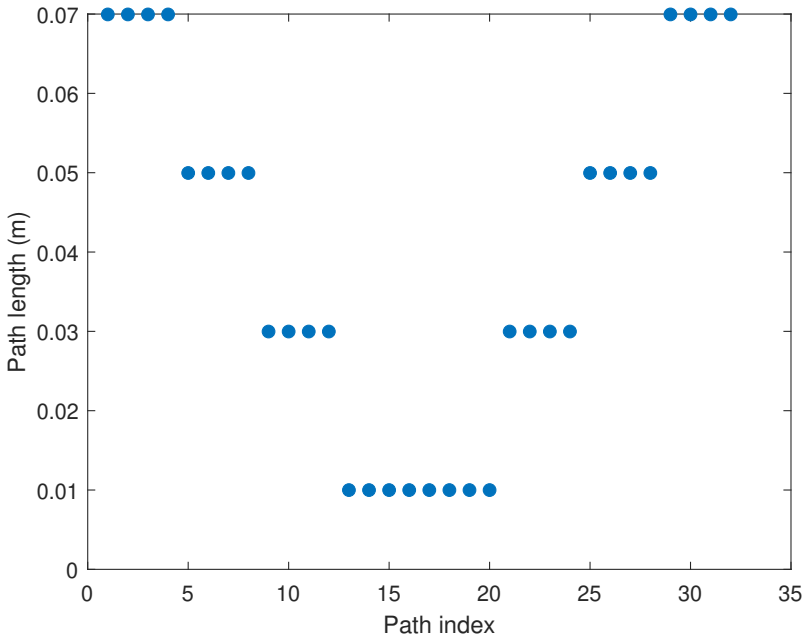

Figure 4.10. Asymmetric path routing with 32 antenna elements, steer angle 0°, beams at different frequencies and with sum node at center element group of 4.

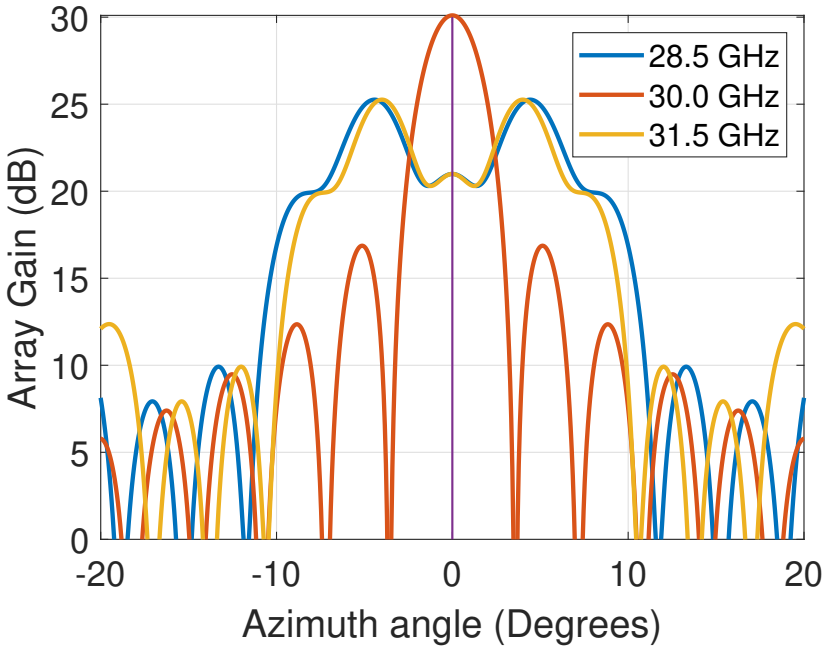

Figure 4.11. Asymmetric path routing with 32 antenna elements, steer angle 0°, beams at 3 different frequencies and with sum node at center element group of 4.

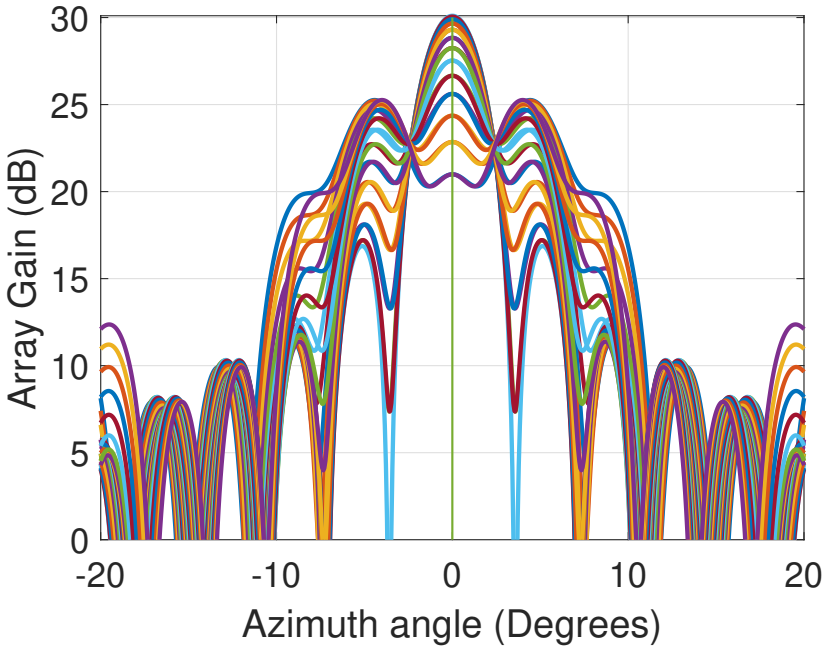

Figure 4.12. Asymmetric path routing with 32 antenna elements, steer angle 0°, beams at different frequencies and with sum node at center element group of 4 with multiple frequency points.

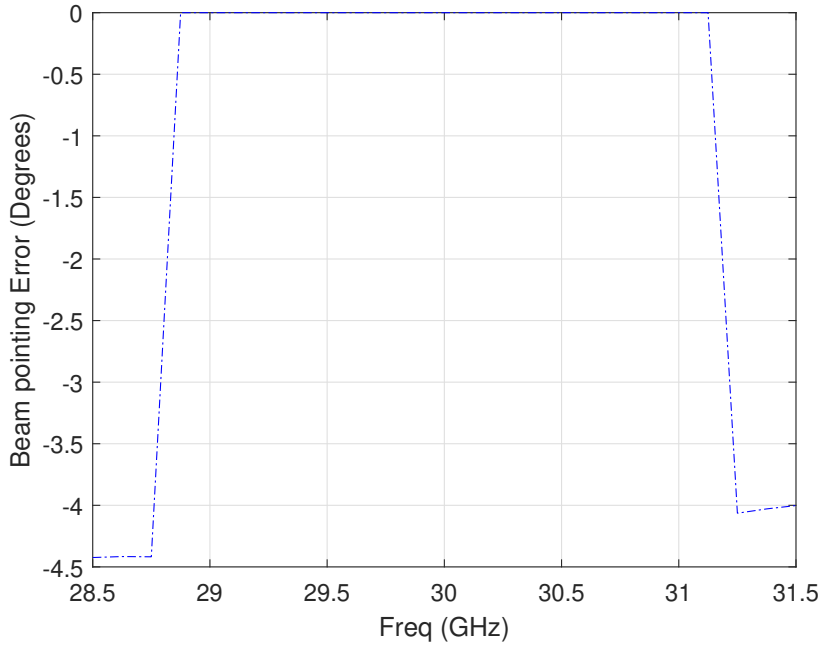

Figure 4.13. Beam pointing error for asymmetric path routing with 32 antenna elements, steer angle 0°, beams at different frequencies and with sum node at center element group of 4.

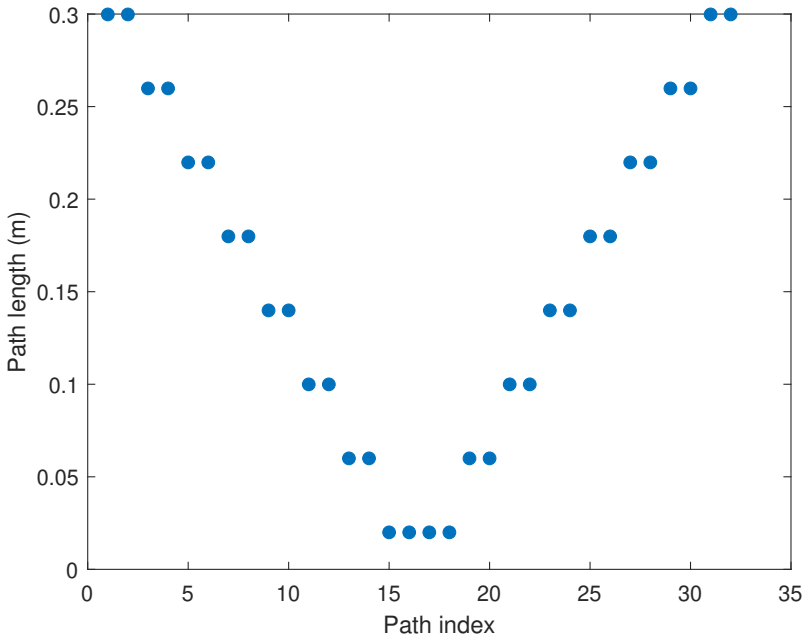

Figure 4.14. Asymmetric path routing with 32 antenna elements, steer angle 0°, beams at different frequencies and with sum node at center element group of 2.

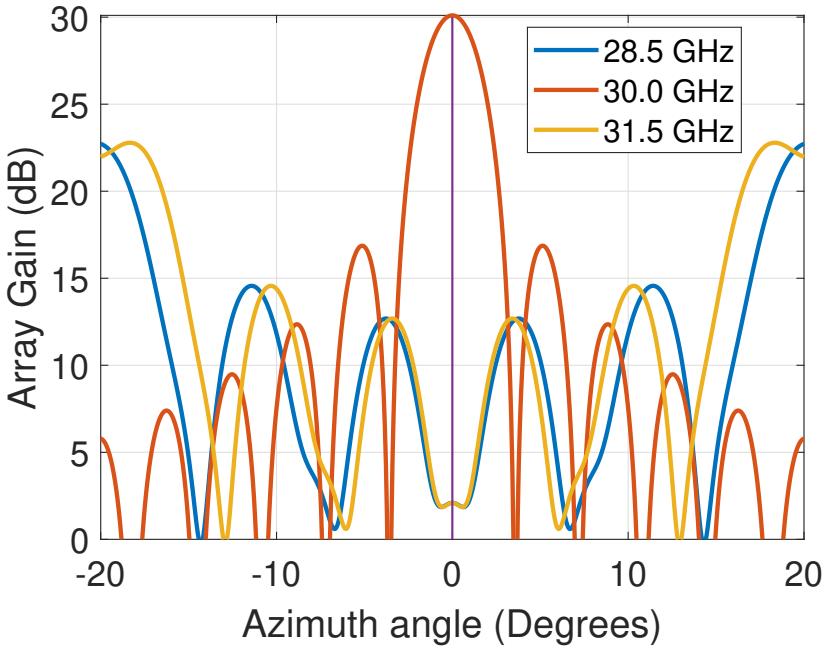

Figure 4.15. Asymmetric path routing with 32 antenna elements, steer angle 0°, beams at 3 different frequencies and with sum node at center element group of 2.

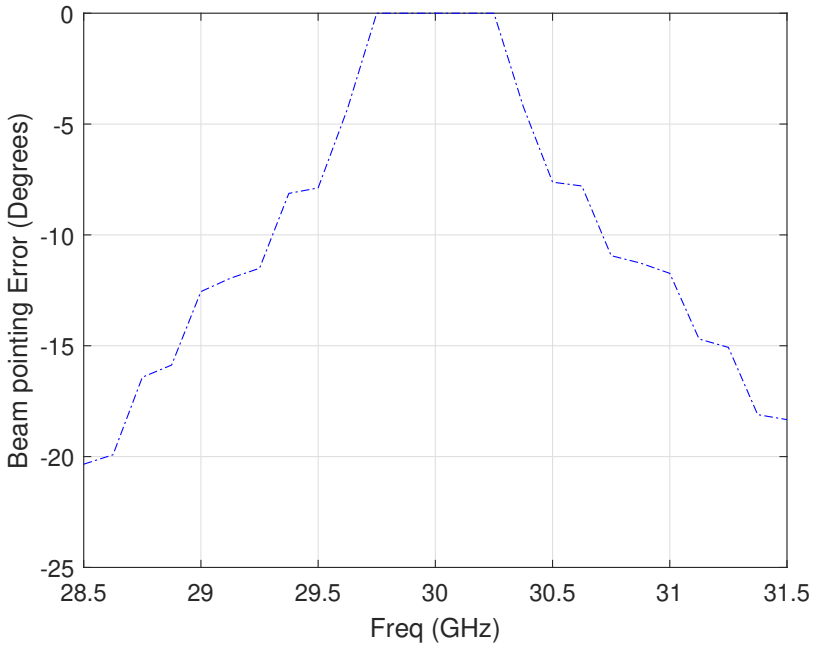

Figure 4.16. Beam pointing error for asymmetric path routing with 32 antenna elements, steer angle 0°, beams at different frequencies and with sum node at center element group of 2.

5 CONCLUSIONS

In this thesis, performance of phased array antennas is analyzed in different scenarios and routing architectures. Receiver side of antennas are modelled, and uniform linear arrays are used with phase shifters connected to each antenna element. The position of the summing node for the antennas is changed to create different path lengths and thus different routing architectures. Beam squint phenomena is observed which constitutes two things: beam pointing error and power loss in the beams. Antenna array size, relative bandwidth and the steering angle are varied to observe how changing these parameters affect the beam squint and thus the performance of the system. Simulations are carried out for array size of 8, 16 and 32 antenna elements, bandwidth percentages of 3% and 10% of 30 GHz and steering angles of 0°, -10°, +10°and +20°. Each parameter is changed while keeping the others constant. These simulations were carried out for a traditional phased array, that is, with symmetric routing.

Changing the array size does not affect the beam pointing error but it does affect the power loss in the system since changing the array size changes the beamwidth. Greater the array size, narrower is the beamwidth. Although it gives the same beam pointing error, power loss is increased because the difference in power between the peak of main lobe and the power at the steering angle increases. Changing the steering angles affects both the beam pointing error and the power loss in the system. At 0°steering angle, its absolute value increases either side of the center frequency. For +10°steering angle, it increases as the frequency in the bandwidth increases and it decreases with -10°steering angle. With an increase in steering angle, power loss decreases. Bandwidth employed in the system also affects the beam pointing error and the power. With a larger bandwidth, beam pointing error is greater but the loss in power is less.

Since the asymmetric configuration has unequal path lengths, it causes delays among the paths and the corresponding beam is formed at a position away from the steering angle. These routing delays are compensated by using phase shifters which enable the beam to form at the position of the steering angle. Asymmetric routing can have indefinite number of possibilities since the concept of asymmetry refers to unequal path lengths.

Changing the architecture brings changes in system performance. Simulations were carried out with different architectures. Simply changing the sum node position in the ULA changes the path lengths and thus the architecture for the simulations were carried out and observations made. A modular approach to the design antenna panels is also carried out where an antenna array is created using smaller groups of antennas. These designs have a high practicality since these groups of antenna elements can be used as packages and these packages can be aggregated to form larger phased arrays. This opens doors for different architecture possibilities and are also feasible since the packages can used in a plug-and-play situation. This work can be extended to 2D arrays of 5G and beyond antenna array systems, which can involve extensive simulation analysis for the optimal feeding systems for the different array architectures.

6 BIBLIOGRAPHY

[1] Agiwal M., Roy A. & Saxena N. (2016) Next generation 5g wireless networks: A comprehensive survey. IEEE Communications Surveys & Tutorials 18, pp. 1617–1655.

[2] Saad W., Bennis M. & Chen M. (2020) A vision of 6g wireless systems: Applications, trends, technologies, and open research problems. IEEE Network 34, pp. 134–142.

[3] Pärssinen, Aarno and Alouini, Mohamed-Slim, and Berg, Markus and Kürner, Thomas and Kyösti, Pekka and Leinonen, Marko, E. and Matinmikko-Blue, Marja, and McCune, Earl and Pfeiffer, Ullrich and Wambacq, Piet (2020) White Paper on RF Enabling 6G - Opportunities and Challenges from Technology to Spectrum [White paper]. (6G Research Visions, No. 13). University of Oulu. URL:`http://urn.fi/urn:isbn:9789526228419`.

[4] Hussain M.T., Sharawi M.S., Podilchack S. & Antar Y.M.M. (2016) Closely packed millimeter-wave mimo antenna arrays with dielectric resonator elements. In: *2016 10th European Conference on Antennas and Propagation (EuCAP)*, pp. 1–4.

[5] Kallnichev V. (07 2001) Analysis of beam-steering and directive characteristics of adaptive antenna arrays for mobile communications. Antennas and Propagation Magazine, IEEE 43, pp. 145 – 152.

[6] Reis J.R., Copner N., Hammoudeh A., Al-Daher Z.M.E., Caldeirinha R.F.S., Fernandes T.R. & Gomes R. (2016) Fss-inspired transmitarray for two-dimensional antenna beam-steering. IEEE Transactions on Antennas and Propagation 64, pp. 2197–2206.

[7] Zhang J., Dai L., He Z., Ai B. & Dobre O.A. (2019) Mixed-adc/dac multipair massive mimo relaying systems: Performance analysis and power optimization. IEEE Transactions on Communications 67, pp. 140–153.

[8] Saha S.K., Garg A. & Koutsonikolas D. (2015) A first look at tcp performance in indoor ieee 802.11ad wlans. In: *2015 IEEE Conference on Computer Communications Workshops (INFOCOM WKSHPS)*, pp. 63–64.

[9] Park S.H., Kim B., Ku Kim D., Dai L., Wong K.K. & Chae C.B. (2022) Beam squint in ultra-wideband mmwave systems: Rf lens array vs. phase-shifter-based array. IEEE Wireless Communications pp. 1–8.

[10] Karabey O.H. (2014) Electronic beam steering and polarization agile planar antennas in liquid crystal technology. Ph.D. thesis.

[11] Muhammad Irshad K., Muhammad A., Muhammad Kabir K., Saeed Ur R. & Aamir S. (2021) A Survey on Beam Steering Techniques in Printed Antennas. International Journal of Recent Contributions from Engineering, Science & IT (iJES) .

[12] Herschel R. & Schaeffer C. (10 2014) Phase modulated radio-over-fiber system for high order modulation millimeter wave link. Lightwave Technology, Journal of 32, pp. 3602–3608.

[13] Haupt R.L. (2019) Lowering the sidelobe level of a two-way array factor for an array with uniform transmit and uniform receive arrays. IEEE Transactions on Antennas and Propagation 67, pp. 4253–4256.

[14] Muhammad Yasir J. (2017) Characterizing nonlinearity in multiantenna multibeam transmitters. (master's thesis). university of oulu URL:http://jultika.oulu.fi/files/nbnfioulu-201712053277.pdf.

[15] Miura R., Oodo M. & Koyama Y. (1998) Maximal-ratio-combining array beamforming assisted by training sequences for sdma mobile radios. In: *IEEE GLOBECOM 1998 (Cat. NO. 98CH36250)*, volume 6, pp. 3204–3208 vol.6.

[16] Fan D., Li Z. & Deng Y. (2008) A study and research of some microwave circuits which bring group delay ripples in broadband communication system. In: *2008 International Conference on Microwave and Millimeter Wave Technology*, volume 1, pp. 112–114.

[17] Leinonen M., Pärssinen A., Shaheen R., Akbar R. & Sethi A. (2020) Configurable antenna arrangements US Patent 16/824,745.

[18] Abdel-Wahab W.M., Al-Saedi H., Raeiszadeh M., Alian E., Chen G., Ehsandar A., Ghafarian N., El-Sawaf H., Palizban A., Nezhad-Ahmadi M.R. & Safavi-Naeini S. (2018) A modular architecture for low cost phased array antenna system for ka-band mobile satellite communication. In: *36th International Communications Satellite Systems Conference (ICSSC 2018)*, pp. 1–5.

[19] Kaare Brandt P. & Michael Syskind P. (2012) The Matrix Cookbook.

7 APPENDICES

7.1 Matlab Script for the simulations

```
%% Simulation parameters
Nz = 32;                              % Total no. of elements
fd = 30e9;                            % Design Frequency
fc = 30e9;                            % Operating Frequency
c = physconst('LightSpeed');          % Speed of Light
c_board = c;
lambda = c/fc;                        % Wavelength
lambda_d = c_board/fd;                % Design Wavelength
d_antenna = lambda_d/2;               % inter-element spacing

Nfreq =1000;
PercentageBW = 10;
PBW = PercentageBW/100;
freqVec = linspace(fc-((PBW*fc)/2),fc+((PBW*fc)/2),Nfreq).';
epsr = 3.3;
mur = 1;
inc = 0.001;
theta = -90:inc:90;                  % Angular space
kd =(2*pi/lambda_d);                 % Design freq wavenumber
kb = 2*pi*sqrt(epsr*mur)./lambda_d;

lambdavect = c_board./freqVec;
kvect =(2*pi*sqrt(epsr*mur)./lambdavect); % Wave Number

%% Routing (including route delays)
% HERE ONE ANTENNA AS REFERENCE ROUTE IS CHOSEN

%DD = abs((d_antenna*[0:1:(Nz-1)])); % unsymmetric
%DD = d_antenna*zeros(1,Nz); % symmetric
%DD = d_antenna*abs([-1:1:(Nz-2)]);
%DD = abs((d_antenna*[-(Nz-1)/2:1:(Nz-1)/2]));
    asubarray = [1 1 1 1];
    Nroutes = Nz/numel(asubarray);
    aroutes = abs([-(Nroutes-1)/2:1:(Nroutes-1)/2])*Nroutes/2;
    DD = d_antenna*kron(aroutes,asubarray);

Hroute = exp(1i.*kvect*DD);  % routes modeled as freq dependent
Hpsroute0 = exp(-1i.*kb.*DD);% phase shifters modeled as phase
Hpsroute = repmat(Hpsroute0, Nfreq,1);

Hroutecomp = Hroute.*Hpsroute;


%% Beamforming
Steer = 0;
ProgPhases = reshape(kd*d_antenna*sind(Steer), numel(Steer), 1);
```

```
Wrf = [exp(-1i.*ProgPhases*(0:1:(Nz-1)))];

%% AF calculation

AFmrt_comp = zeros(numel(freqVec),numel(theta));
for ind = 1 : numel(freqVec)
    ProgPhasesAF = reshape(2*pi*(freqVec(ind)/c)*d_antenna*sind(theta),...
    numel(theta), 1);
    Haf = [exp(1i.*ProgPhasesAF*(0:1:(Nz-1)))].';
    AFmrt_comp(ind,:) = (Hroutecomp(ind,:).*Wrf)*Haf;
end
%% calculating Squint and Power loss
[simsteer,Steer_index] = min(abs(Steer - theta)); % index at steering angle
for freq = 1 : Nfreq
    f = AFmrt_comp(freq,:); % extracting each row of whole matrix

    % peak value and its index of each frequency
    [peak_value,peakIndex] = max(abs(f));
    peak_angle = theta(peakIndex);
    Squint(freq,:) = abs(Steer) - abs(peak_angle);

    % pwr at steer angle for every frequency
    PWR_Steer = abs(AFmrt_comp(freq,Steer_index));

    PWR_loss(freq,:) = PWR_Steer./peak_value;
end

%% Plotting
y_min = 0;
y_max = 20*log10(Nz);
y_limit = y_min:y_max;

%% main plot
figure;
hold on;

for pInd = 1: Nfreq
    plot(theta, 20*log10(abs(AFmrt_comp(pInd,:))),'Linewidth',2)
end
plot(Steer(1)*ones(size(y_limit)),y_limit,'Linewidth',1)
hold off;
grid on;
set(gca,'FontSize',16)
box on
xlim([-20 20])
ylim([y_min y_max])
xlabel('Azimuth angle (Degrees)')
ylabel('Array Gain (dB)')
legend ('28.5 GHz', '30.0 GHz', '31.5 GHz')
```

```
%% plotting Beam pointing error
figure;
hold on;
plot(freqVec/1e9, Squint,'-.b','markersize',12)
xlabel("Freq (GHz)");
ylabel("Beam pointing Error (Degrees)");
grid on;
box on;
hold off
set(gca,'FontSize',11)

%% plotting power loss
figure;
hold on
plot(freqVec/1e9,20*log10(abs(PWR_loss)),'-xk')
xlabel("Frequency (GHz)");
ylabel("Power loss (dB)");
grid on
hold off
set(gca,'FontSize',14)

%% plotting path lengths for antenna elements
figure
plot(1:Nz, DD, '.', 'MarkerSize', 20);
xlabel("Path index");
ylabel("Path length (m)");
```